Investigation of the adhesive from *Hormosira banksii* germlings and its performance over different material surfaces and topographies

Simone Dimartino[1,2,*], Anton V. Mather[3], Jock S. Nowell-Usticke[1], Brendon Fischer[1], Volker Nock[2,4]

[1] Department of Chemical and Process Engineering, [2] Biomolecular Interaction Centre, [3] Department of Biological Sciences, [4] Department of Electrical and Computer Engineering University of Canterbury, Private Bag 4800, Christchurch, New Zealand

* Corresponding author: simone.dimartino@canterbury.ac.nz

Abstract

Adhesives produced by marine organisms possess the ability to adsorb robustly and under water to a range of substrates, in a range of environmental conditions and undergo curing under water. In the present work, the bioadhesive produced by germlings of a large brown seaweed, *Hormosira banksii*, is investigated to assess its adhesive performance. The production of the adhesive secretions was monitored using microscopy and staining experiments, while the attachment strength over substrates of varied chemistry and topography was indirectly evaluated through flow channel experiments. *H. banksii* germlings displayed a two-stage development of the adhesive, with an initial uniform production around the entire germling, followed by localized production in the rhizoidal tip. Germlings were found to exhibit a settlement-time dependent increase in adhesion strength across all of the substrates investigated, including glass, stainless steel, poly(methyl methacrylate) (PMMA), polytetrafluoroethylene (PTFE) and polydimethylsiloxane (PDMS). Conversely, any substrate-dependent variation in the adhesive strength was not observed, suggesting *H. banksii* germlings are able to produce an adhesive able to interact with a range of substrate types. On substrates with simple, defined topographies, *H. banksii* zygotes were found to adhere most effectively to a surface with a feature size slightly larger than the size of the zygote. A feature size smaller than the zygote resulted in a minor disruption of adhesion strength that diminished with settlement time.

Keywords

Bioadhesives, macroalgae, *Hormosira banksii*, flow channel, microscopy, adhesion.

1. Introduction

Many aquatic organisms like mussels, barnacles and algae have seemingly no problem achieving strong adhesion in wet environments (Petrone, 2013; Stewart et al., 2011). On the other hand, the challenge of achieving long-lasting, robust adhesion in a wet environment remains elusive to today's engineers. Applications for wet-resistant adhesives are numerous, from biosensors to aquaculture and underwater construction (Lee et al., 2007). In particular, biologically inspired adhesives are potentially biocompatible, with promising biomedical applications such as for repairing damaged tissues, sealing blood vessels and cementing bones (Haller et al., 2011).

Understanding the interactions between biological adhesive compounds and their substrates is the first step in the design of synthetic adhesives. However, the study of bioadhesives from marine organisms is very challenging, with an extremely complicated formulation containing post-translationally modified proteins, glycoproteins, polyphenols and polysaccharides (Bitton et al., 2006; Endrizzi and Stewart, 2009; Hennebert et al., 2012; Tarakhovskaya, 2014; Waite and Qin, 2001)). They are also, by necessity, largely insoluble, undergo rapid curing processes, and are often produced in very small quantities (Santos et al., 2013). For these reasons, extraction and purification of marine bioadhesives for chemical analysis is difficult (Jordan and Vilter, 1991; Levi and Friedlander, 2004), and many indirect techniques including microscopy (optical (Fagerberg et al., 2012; Ouriques et al., 2012) SEM (Apple et al., 1996; Callow et al., 1978; Moss, 1975), ESEM (Callow et al., 2003), TEM (Bråten, 1975; Ouriques et al., 2012; Petrone et al., 2011) and AFM (Chiovitti et al., 2008; Walker et al., 2005; J. A. Callow et al., 2000), quartz crystal microbalance with dissipation (Molino et al., 2008, 2006), zeta potential (Rosenhahn et al., 2009), spectroscopy (EDX (Petrone et al., 2011; Chiovitti et al., 2008) and IR (Barlow and Wahl, 2012; Petrone et al., 2011)) and enzymatic assays (Apple and Harlin, 1995; Pettitt et al., 2004), are often employed. Among them, staining is a relatively easy tool to identify or rule out the main molecular classes present in the adhesive, as well as help follow the production of the adhesive with time (Ouriques et al., 2012; Apple et al., 1996; Bouzon and Ouriques, 2007).

The limited amount of adhesive produced by marine organisms and the difficulty in performing dedicated testing strongly restricts mechanical characterization. For this reason, it is often preferred to assess the attachment strength of whole organisms in appropriate flow channels as a proxy method to determine the strength of the bioadhesive (Arpa-Sancet et al., 2012; Hodson et al., 2012; Schultz et al., 2000). Flow channels offer the opportunity to test adhesion of marine organisms *in-situ* and *in-vivo*, and help in selecting appropriate species to

be used as inspiration for biomimetic glues. Flow channel experiments are also useful in the biofouling arena, in particular for the testing of new low-fouling or self-cleaning materials, e.g. surfaces displaying hydrophilic/hydrophobic characteristics (Bauer et al., 2013; Chapman and Regan, n.d.) or textured surfaces (Callow et al., 2002; Myan et al., 2013).

Among the various marine organisms, large seaweeds are able to form strong, underwater, irreversible and long-lasting attachment, well able to endure the severe hydrodynamic forces present in marine environments (Harder et al., 2006; Seymour et al., 1989). In particular, *Hormosira banksii* (Turner) Decaisne thrives in the intertidal zone, i.e. where forces associated with wave action and tidal currents are the highest, making the adhesive produced by this species particularly interesting (McKenzie and Bellgrove, 2009). Algae-based adhesion is preferentially studied using spores (James A Callow et al., 2000; Callow and Callow, 2006), zygotes (Taylor and Schiel, 2003) or germlings (Norton, 1983; Taylor et al., 2010), mostly because attachment must rely on chemical interactions only rather than mechanical interlocking as for adult specimens. In particular, zygotes and germlings of *H. banksii* have been recently used to determine the attachment behavior over different surfaces of biomedical relevance (Dimartino et al., 2015), while infrared spectroscopy has been employed to inquire on its adhesive formulation (Dimartino et al., submitted to The Journal of the Royal Society Interface).

In the present work, staining with toluidine blue and flow channel experiments are employed to study the mechanism of attachment and detachment of *H. banksii* germlings, as well as the process of production of the adhesive mucilage. Flow channel experiments are also employed to determine the performance of the adhesive over different substrates of industrial relevance, namely glass, stainless steel, poly(methyl methacrylate) (PMMA) and polytetrafluoroethylene (PTFE). The flow channel was also employed to evaluate the effect of different topographies on germling settlement and attachment.

2. Materials and Methods

2.1. Sample collection and preparation of gamete suspensions

The procedure employed to harvest suspensions of gametes from *H. banksii* reflects the protocol described by Dimartino *et al*. (Dimartino et al., 2014). Briefly, *H. banksii* plants were collected from Pile Bay, Lyttelton Harbour (43°37’13.6”S, 172°45’38.7”E) at different times comprised between October 2013 and January 2015, transported in a chilly bin and thoroughly washed with 0.2 μm filtered and UV-treated seawater. Plants were stored

separately in plastic bags and kept in the dark at 4 °C for a period of between 12 and 48 h, followed by thermal and light shock treatment using 2 halogen portable floodlights (500 W each) to stimulate gamete release. Sex of the gametes released is determined by visual inspection of the exudates, namely orange and olive brown for male and female gametes, respectively. Gametes were harvested by washing the plant in separate reservoirs containing sterile seawater at 13 °C. The suspensions obtained were filtered through plankton nets (mesh size was 105 and 25 µm for eggs and sperm, respectively) and further clarified by three subsequent sedimentation cycles under gravity. At all times, plants, labware and suspensions were carefully manipulated to avoid premature contact of eggs and sperm leading to uncontrolled fertilization.

2.2. Cultures of germlings

H. banksii zygotes were produced by mixing the two gamete suspensions for around 30 min, and the concentration of the zygote suspension was adjusted to approximately 20,000 zygotes per ml. 5 ml of the zygote suspension was then inoculated onto the different substrates and settled under gravity. The resulting cultures were placed in separate trays in a temperature controlled chamber at 15 °C with 12 h:12 h light:dark cycles, light intensity of 40 µmol photons m^{-2} s^{-1} of photosynthetically active radiation. Seawater was replaced every 24 h to maintain constant levels of nutrients and oxygen in the culture. From here on, fertilized eggs will be termed zygotes, while zygotes that have attached to a substrate will be referred to as germlings.

2.3. Substrates for adhesion tests

75 x 15 mm slides made of glass (standard microscope slides from Sigma Aldrich, NZ), polished stainless steel (304 grade, Anzor, Christchurch, NZ), PMMA and PTFE (both from Dotmar, Christchurch, NZ) were used for testing the adhesion strength of *H. banksii* germlings. The slides were thoroughly cleaned and equilibrated in seawater for at least 24 h in 0.22 µm filtered and UV treated seawater before inoculation with zygotes.

2.4. Topography design and preparation of patterned PDMS testing slides

Repeating, square bottomed grooves, orthogonal to the flow direction, were chosen as the basis for the topographical substrate design. The grooves produced had uniform depth (27 µm) and varying widths (flat control, 40, 80 and 160 µm), covering an area of 40 mm x 3.5 mm, appropriate to fit in the centerline of the flow channel. Polydimethylsiloxane (PDMS)

slides were prepared using photo-lithography and PDMS casting techniques. Briefly, negatives of the three topographies were first created using SU-8 2025 (MicroChem, Westborough, USA), a negative tone photoresist set on a 4" silicon wafer. Masks were designed in EDA-software (Tanner L-Edit, Mentor Graphics, Wilsonville, USA) and printed on 4" chrome-on-glass masks (Nanofilm, Westlake Village, USA) using a laser mask writer (μPG101, Heidelberg Instruments, Heidelberg, Germany). SU-8 photo-resist was applied to a silicon wafer with a thickness of 27 μm by a two-step process (500 rpm for 10 s, followed by 3000 rpm for 30 s) on a spin-coater (WS-400-6NPP, Laurell Technologies, North Wales, USA). The wafer was then soft-baked for 3 min at 65 °C and 5 min at 95 °C on a contact hot plate. A mask aligner (MA-6, Suss Microtec, Garching, Germany) was then used to expose the photoresist through the mask using UV light. Followed by baking for 1 min at 65 °C and 5 min at 95 °C and immersion in developer (Propylene glycol monomethyl ether acetate, Sigma-Aldrich, NZ) to remove non-cured SU-8, thus leaving a series of raised rectangular blocks which formed the negative for creating the grooves in the silicone slides. The molds were then treated with trimethylchlorosilane (TMCS, Sigma-Aldrich, NZ) prior to addition of the PDMS mixture. Sylgard 184 silicone (Dow Corning, MI, USA), a two part elastomer, was prepared at a ratio of 10:1 w/w base-to-curing agent. The PDMS mixture was degassed under vacuum in a desiccator for at least two hours before being poured into the mold to a depth of approximately 3 mm. The PDMS and mold were placed under vacuum in a desiccator to further degas the PDMS and facilitate filling. The PDMS was removed from the vacuum and baked for 2 h at 80 °C on a contact hotplate before being removed from the mold after which was placed between polyethylene sheets and baked for a further 2 h at 80 °C to complete curing. The cured PDMS castings containing three topographical strips were cut into three approximately microscope slide-sized pieces (20 mm x 75 mm) to fit in the flow channel. Before inoculation with the cultures, the PDMS slides were oxygen plasma treated for 12 s at 100 W (Emitech K1050X, Quorum Technologies Ltd., UK) to increase its hydrophobic characteristics. Clean dried slides were soaked for at least 24 h in 0.22 μm filtered and UV treated seawater before inoculation with zygotes.

2.5. Contact angle measurement

Contact angle measurements were performed using a goniometer equipped with high speed camera (CAM200; KSV Instruments Ltd, Helsinki, Finland). Advancing contact angles (θ_{AW}) were taken following deposition of a 2 μl droplet of deionized water on the various surfaces. 10 images of the water droplet, spaced 6 s apart, were taken following a 30 s delay after initial

deposition of the water droplet. The ten images were analyzed using the associated goniometer software (KSV CAM Software v 4.01), which fits the droplet shape to the Young-Laplace equation. The average contact angle was then calculated across the ten images and this average represented the contact angle measurement for a single replicate. Contact angle measurements were performed four times on each substrate and a final average was obtained from these four measurements.

2.6. Atomic force microscopy

The surface roughness of the substrates was estimated using atomic force microscopy (AFM). Scans were performed using a Digital Instruments Dimension 3100 on tapping mode on a scan area of 100 µm x 100 µm and scan rate of 0.1 lines s^{-1}, and scans were taken in triplicate from three randomly selected spots on single slides of each material type. AFM data were analyzed using NanoScope Analysis (version 1.40). Flattening and plane fitting were performed prior to estimation of the roughness.

2.7. Flow channel experiments

Germling survival on three replicates of the four substrate materials (Glass, PMMA, PTFE, Stainless Steel) and the four PDMS topographies (40, 80, 160 and control) was assessed after settlement times of 12, 24, 48 and 96 h. The flow channel was operated as described in Dimartino et al. (Dimartino et al., 2015). Briefly, the slides were clamped into the flow channel and exposed to stepwise increases in the flow rate, from 0 to 2.50 m s^{-1} (300 ml min^{-1}), in seven even steps each lasting 15 s. Videos of germlings in the flow channel were obtained at 3.5x magnification using a 1.3 megapixel USB CMOS camera (ODCM0130C; ProSciTech, Townsville, Australia) controlled using ToupView (x64 v3.7.1691) and connected to a Nikon SMZ-1B dissecting microscope (Nikon Corporation, Tokyo, Japan). VLC Media Player (v. 2.1.3) was then employed to extract single frames from the beginning of the experiment and at the end of each flow step. Germling numbers were counted in each frame, and germling survival was calculated using: $S_v = D_v/D_0$, where S_v is the survival at the end of flow step at velocity v, D_v is the surface density (germlings per mm^2) at the end of flow step at velocity v, and D_0 is the density at the beginning of the flow channel experiment.

2.9. Staining Procedure

A solution containing 1% toluidine blue and 1% borax in seawater was used for staining. Cultures at 6, 12, 24, and 96 h post fertilization were gently rinsed in seawater and then

covered with 5 ml staining solution for 5 minutes, then rinsed again with seawater. The stained cultures were observed under a compound microscope (Nikon model SE, Tokyo, Japan) equipped with a 1.3 megapixel USB CMOS camera (ODCM0130C; ProSciTech, Townsville, Australia) controlled using ToupView (x64 v3.7.1691). Control slides containing either unfertilized eggs or sperm were also stained and observed under the optical microscope.

3. Results

3.1 Staining experiments

In Figure 1 are reported microscopic images of *H. banksii* germlings stained with toluidine blue at different developmental stages. Toluidine blue effectively stained the cultures metachromatically, with dark blue color in the cytoplasm and other internal organelles of the germlings and vibrant purple/violet for the secreted adhesive materials. Stained extracellular polysaccharides (EPS) are not visible after 6 h fertilization (Figure 1A), they appear after 12 h hours as a slim halo (7 ± 2 µm thick) uniformly surrounding the germlings Figure 1B) which thickens with time up to 27 ± 3 µm at 24 h after fertilization (Figure 1C). Between 24 h and 96 h the germlings polarize and, following cell division, form a protrusion which later develops in the attachment rhizoid. The image at 96 h displays an abundance of stained EPS around the rhizoidal tip (43 ± 5 µm thick) and a thinner mucilage layer surrounding the apical head (20 ± 2 µm thick), indicative of a shift in the production of the adhesive towards in the rhizoid (Figure 1D). Control slides containing unfertilized eggs did not stain, indicating that production of adhesive extracellular polymeric substances only occurs after fertilization.

3.2. Influence of material substrate on adhesion of *H. banksii* germlings

The surface roughness and contact angle were measured for the four substrates considered, namely glass, stainless steel, PMMA and PTFE. In this work, the roughness, R, is defined as the distance between the highest and lowest features on a sample as evaluated through AFM scans, thus representing a conservative overestimation for the size of the irregularities present on a surface. As summarized in Table 1, glass had the lowest roughness, followed by stainless steel and PMMA, while PTFE was the only surface to exhibit a roughness greater than 1 µm. Table 1 also reports the advancing contact angles, θ, for all surfaces, with glass, stainless steel and PMMA exhibiting hydrophilic surface character while PTFE distinguished by its hydrophobic character.

Table 1: Roughness, *R*, and advancing contact angle, θ, measured on the four substrates.

Substrate	*R* (nm, ± SE, n = 3)	θ (± SE, n = 4)
Glass	225 ± 7	57° ± 2°
Stainless steel	412 ± 56	57° ± 2°
PMMA	857 ± 245	74° ± 5°
PTFA	1236 ± 101	103° ± 1°

The initial settlement density of *H. banksii* germlings depended significantly on settlement time ($p < 0.01$, Figure 2). A smaller yet statistically significant variability of initial density upon substrate is also present ($p = 0.014$), particularly at later times where settlement to stainless steel is relatively poor compared to the other substrates.

Survival data of the flow channel experiments are plotted in Figure 3. Note the wall shear pressure, τ_w, is also reported, which, for a Newtonian fluid in laminar flow within a rectangular flow channel, is calculated as $\tau_w = 6\ \nu\ \mu\ /\ h$, where μ is the viscosity of seawater (1.308×10^{-3} Pa s (R. A. Cox, 1970)) and h is the height of the flow channel (0.5 mm). In general, a steep decrease in the survival is observed at low flow rates, i.e. at the beginning of the flow experiments, with fewer germlings being displaced by the flow at higher flow rates. Consistent with the observations for the initial density, most germlings are easily washed out by the hydrodynamic flow. In particular, practically all germlings from the 12 h old cultures are displaced at the end of the experiment, irrespective of the substrate material. The data for older cultures show that an increasingly higher portion of the settled germlings is able to establish a secure attachment to the substrate, withstanding even the highest shear pressure tested. As the starting conditions (in terms of D_0) are not consistent across the experiments, analyses on the complete survival data set such as ANOVA are not of statistical significance. However, one can observe that differences in survival are larger at the conclusion of each experiment, i.e. after exposure to the highest flow rate, thus $S_{2.5}$ was chosen as a qualitative estimator to compare adhesion strength of *H. banksii* germlings across the substrates tested (Figure 4). The $S_{2.5}$ data indicate that glass and PMMA performed consistently better than PTFE and stainless steel at all settlement times tested. Also, it can be observed that survival progressively increases with settlement time, with a trend that appears to continue beyond the 96 h limit tested.

3.4. Influence of topography on adhesion of *H. banksii* germlings

Topographies with groove widths on the same scale as *H. banksii* zygotes were manufactured, namely 0 (control), 40, 80 and 160 μm, corresponding to ½, 1 and 2 zygote diameter approximately. All grooves were 27 μm deep (⅓rd of zygote diameter) and separated by 40 μm wide ridges. Even though the attachment performance of *H. banksii* germlings does not seem to be influenced by surface energy, it is common belief that hydrophilic surfaces foster adhesion. For this reason, the native hydrophobic PDMS surfaces (contact angle of 104.0° ± 1.5°, n = 12) were oxygen plasma treated, with a resulting contact angle of 66.9° ± 3.7° (n = 12).

Figure 5 shows the location of the settled germlings on the different topographies tested after a settlement time of 24 hours and before flow channel exposure. While germlings randomly colonized the control surface, distinct patterning was clearly visible on the various topographies, with germlings preferentially occupying the grooves. Germlings also settled on the ridges between grooves, particularly on the 40 and 80 μm surfaces (circles in Figure 5), often as part of a germling cluster. The relatively small groove depth allows approximately 2/3 of the groove-settled germlings to protrude, creating new useful topographical features for ridge-settled germlings.

Figure 6 shows average starting densities (D_0) for the four topographies considered at different settlement times. Two-way ANOVA confirmed a significant difference in starting density as a result of settlement time ($p < 0.05$), but no significant variation as a result of topography ($p = 0.18$). Comparison of D_0 within each topography indicated that the initial germling density stabilized after 24 hours with no significant difference between 24 and 48 hour ($p = 0.27$). Also in this case, the different initial germling density impeded to conduct solid statistical analyses on the results of the flow channel experiments. Still, sound qualitative considerations can be put forth. In particular, increase in survival with settlement time is more than apparent (Figure 7), with the 80 μm grooved surface exhibiting the highest survival rate under the entire range of flow velocities investigated and at any settlement time. Of the remaining topographies, there is no clear poorest or best performer in terms of germling survival.

4. Discussion

The metachromasia in the samples stained with toluidine blue is consistent with the presence of strongly acidic EPS containing sulfate and phosphate groups (Sridharan and Shankar, 2012). Negatively charged polysaccharides bearing sulfate groups have been detected for this species using infrared spectroscopy (Dimartino et al., submitted to The

Journal of the Royal Society Interface), with relevance both in the cohesive and adhesive process. The charged sulfate moiety is in fact able to form strong interactions with various metals and metal hydroxides, as well as prone to cross-link through coordination bonds in the presence of dissolved metal ions. The progressive production of adhesive materials, as stained by toluidine blue, is relatively slow, mirroring the relatively slow growth rate of the germlings (Osborn, 1948). It has been experimentally observed that settled germlings of *H. banksii* are able to establish a secure attachment to a substrate only after approximately 24 h following fertilization (Dimartino et al., 2015; Taylor et al., 2010), i.e. when a relatively copious amount of EPS has been discharged in the external environment. It is also possible that slow kinetics of cross-linking reactions of the EPS influences the time required for safe attachment (Vreeland and Epstein, 1996).

Glass, stainless steel, PMMA and PTFE were selected as model materials to study the attachment of the adhesive EPS from *H. banksii* germling. Their widespread use in a plethora of research and industry applications, as well as their very different chemical, physical and mechanical properties make them appropriate candidates for this study.

The silicate base of glass is similar to the structure of silicate rocks, and can be considered as a chemical approximation of inorganic rock substrates present in marine environments. PMMA is a biocompatible material widely used in biomedical applications such as in intraocular lenses, bone cements and dentures (Frazer et al., 2005). The excellent mechanical characteristics of PMMA together with its low cost grant it widespread use in a plethora of applications in research and industry (Hong et al., 2010; Weaver et al., 1993). Polytetrafluoroethylene (PTFE) is a hydrophobic non-stick material with excellent chemical and mechanical properties, mostly used as antifouling and corrosion-resistant coating. Finally, stainless steel is used in a wide range of applications, including biomedical, food and chemical processing, and structural and naval engineering.

The surface roughness measured on the substrates tested was in all cases at least one order of magnitude lower than the size of *H. banksii* germlings, approximately measuring 70 µm in diameter. Even though some features of the adhesives might benefit from local textures on the nanoscale (Granhag et al., 2004), macroscopically the different adhesion behavior over the various substrates is mainly related to the chemistry and physics of the interaction of the adhesive with the surface rather than mechanical interlocking or hydrodynamic protection effects. In terms of wettability characteristics, glass, stainless steel and PMMA displayed strong hydrophilic properties, while PTFE was strongly hydrophobic. The surface of glass is hydrophilic due to the abundance of hydroxyl functional groups able to form hydrogen bonds

with water molecules. Metal ions present on the stainless steel surface readily interact with polar solvents such as water, while surface bound hydroxyl groups belonging to metal-hydroxides can be involved in hydrogen bonding, furthering its hydrophilic behavior. PMMA also displays a number of polar moieties able to interact with water molecules. On the other hand, the hydrophobicity of PTFE is mainly associated to its highly fluorinated backbone. While the hydrophilic/hydrophobic character of the surfaces are mainly explained by surface chemistry, e.g the abundance/lack of polar functional groups, it is curious to note a correspondence between contact angles and roughness, in that substrates with higher roughness are less hydrophilic. While this does not necessarily imply causation, topography and chemistry have both been implicated in surface wettability (Onda et al., 1996; Sun et al., 2005). Overall, the four materials considered span a good range of surface properties appropriate to test the flexibility of the adhesive produced by *H. banksii* germlings.

Differences in the initial density suggest that the germlings have not yet secured to the culture substrates at early times (12 and 24 h) and are strongly subject to wash-out effects when the slides are transferred from the culture trays to the flow channel. A strong base-level of adhesion is achieved within the first 48 h after settlement, a slightly longer time than the 24 h observed in previous experiments (Dimartino et al., 2015) or in the topography experiments. This result further confirms the microscopic observations and the strong link between the amount of EPS produced and attachment strength. Differences in the time required to achieve strong attachment was assigned to biological variations in the samples collected.

The flow channel experiments suggest that *H. banksii* attachment is somewhat more performant on glass and PMMA substrates, while displays lower adhesion on stainless steel and PTFE. Given the different performance of glass and stainless steel, despite identical contact angles, it seems unlikely that wettability is the primary determinant for adhesion strength. Similarly, the possibility that the higher roughness of the PTFE surface is responsible for its low survival rate seems contradicted by the relatively high adhesion to PMMA (second roughest substrate) and low survival on stainless steel (second smoothest substrate). Preliminary results obtained from similar experiments carried out with *Durvillaea antarctica*, another seaweed belonging to the Fucales and closely phylogenetically related to *H. banksii*, reveal some interesting discrepancies (Anton V. Mather, Development of a Novel Flow Channel Apparatus and its Use in Testing the Adhesion Strength of Two Common New Zealand Algae, PhD Thesis, University of Canterbury, 2015). In fact, stainless steel appears to produce highest survival rates of *D. antarctica* germlings at all settling times tested (6, 12 ,24 and 48 h), but had the lowest survival rates for *H. banksii* germlings. The mechanism of

adhesion responsible for *D. antarctica*'s rapid adhesion to the substrate may involve some interaction with metal ions or oxides that the *H. banksii* adhesive is not only not capable of also exploiting, but might be involved to some extent in attenuating its adhesive strength. On the other hand, both initial density and survival of *H. banksii* germlings settled on the different surfaces have similar magnitude, indication that the adhesive produced is multifunctional and able to adapt to different materials, with comparably good performance even on the anti-stick PTFE. Such adaptable attachment behavior was observed on other marine species such as mussels (Suci and Geesey, 2001) and barnacles (Luigi Petrone, 2011). Many algal motile spores swim and probe the surface prior to settlement, with a rigorous selection process on the preferred locations dictated by a number of cues such as light, topography, as well as other surface properties of the substrate (Callow et al., 2002; Long et al., 2010; Rosenhahn and Sendra, 2012). On the other hand, *H. banksii* oogotes and germlings are non-motile, and thus cannot select a location to settle and therefore need to secure themselves well to a variety of substrates. The results here discussed suggest an evolutionary development of a versatile adhesive to offset the impossibility to select a preferred location on a substrate. The flexibility of the adhesive from *H. banksii* highlights the opportunity offered by this seaweed species to develop a new multipurpose and water-resistant biomimetic glue.

Overall, the adhesion of the germlings to the substrate appeared to take place in two stages. A first adhesion stage occurs immediately after fertilization, where the adhesive material present on the surface of the new zygote comes into contact and forms an initial bond with the substrate. As the germling develops and the rhizoid grows, the location of adhesion migrates to the rhizoid tip while the adhesive bond between the germling body and the substrate weakens. This reflection is consistent with the staining experiments, i.e. the observed abundant production of EPS around the rhizoidal tip with a contemporary reduction of the mucilage surrounding the apical head. This transfer of adhesion locus from germling body to rhizoid tip allows the germling body to move away from the substrate and lift higher into the water body. Evidence for the transfer of attachment point to the rhizoid as germlings aged was observed as a change in the way the germlings were removed from the surface during adhesion testing. Using the video footage recorded during the experiment it was noted that younger germlings (6, 12 and 24 hours old), which did not exhibit much rhizoid development, tended to detach in a single event. However, for older germlings (96 hours) with a somewhat developed rhizoid, it was noted that, in some instances, adhesion between the germling body and the substrate was disrupted first and followed by the detachment of the rhizoid. On video this appeared as the free moving germling body rotating about the tip of the rhizoid which

remained stationary (Figure 8). This observation at 96 hours post-settlement indicates that the transfer of adhesion locus occurs sometime between 24 and 96 hours, signifying the start of the next step in the germling's life story where it begins to grow out into the water body for better nutrient access and waste removal. This behavior was shared across the different materials, further indication that the attachment mode is not influenced by surface properties and highlighting the versatility of the adhesive from *H. banksii* germlings.

Starting density was lowest after 12 hours settlement, mainly due to limited production of the adhesive and easy detachment of the germlings during transfer of the slides to the flow channel. Initial density clearly increased at 24 hours and stabilized afterwards for all topographies, indicating the establishment of a firm adhesion to the substrate. This result suggests that germlings in this batch of experiments were quicker in securing themselves to the substrates, in agreement with previous experiments on different material surfaces (Dimartino et al., 2015). Even if zygotes are non-motile, most germlings developed within the textured channels. This is due to the narrow design of the ridge separating the grooves thus impeding stable settlement. Nevertheless, germlings are also found on ridges when in close proximity to several groove-settled germlings, i.e. where they benefit from cooperative mucilage/adhesive production as well as some degree of hydrodynamic protection.

As expected, the flow experiments reveal that highest survival was obtained with the 80 µm textures surface. Such topography easily accommodates the zygotes and protects them from hydrodynamic stresses. Also, the proximity of the side walls in addition to the groove floor provides three theoretical points of adhesive contact, further fostering settlement (Scardino et al., 2006, 2008). The seemingly similar survival recorded for the three remaining topographies can be explained through both geometric considerations, as well as the attachment point theory. *H. banksii* germlings are surrounded by a strong carbohydrate based cell wall that helps maintaining their spherical shape (Forbes and Hallam, 1979). Figure 9 is a simplified schema of the settled germlings over the different sized grooves, showing that germlings over the flat, 40 and 160 µm grooved topographies are protruding similarly from the floor of the flow channel and are likely subjected to similar hydrodynamic stresses. In addition, germlings over the 40 µm grooved topography have two contact points of attachment, as also often occurs for germling settled on the edge of the 160 µm surface. While the flat PDMS cast offers only one attachment point for the germlings, this deficiency is well compensated by random clustering and gregarious settlement behavior which fosters cooperative interaction between the germlings. It is worth noticing that germlings on the 160 µm topography often fill the grooves in pairs of lines, thus creating an additional, but shared,

contact point. The lower attachment efficiency of germlings on the 160 µm topography with respect to the 80 µm topography highlights that this shared attachment point is not as effective for adhesion as the entire cell cluster can be potentially removed due to the current flow. The importance of hydrodynamic forces on germling detachment over the number of attachment points can also be inferred from the survival rate of groove- and ridge-settled germlings. In particular, ridge-settled germlings detached up to six times more readily than groove-settled germlings on all topographies and at all settlement times. Therefore, even if ridge-settled germlings can leverage on additional attachment points from the vicinal germlings settled in the grooves, the forces resulting from fluid flow on more exposed germlings constitute the main cause of detachment.

This work further confirms the versatility of the adhesive produced by *H. banksii* in its first life stages, with the interesting capability to adhere to a number of different materials surfaces. The time the germlings require to complete attachment and secure themselves to a substrates ranges from 24 to 48 h. Even if this long time may superficially appear as a drawback, we believe this lag is mostly associated with the slow rate of cellular production and release of the adhesive secretions in the external environment. Future work will be devoted to prove the hypothesis that it is the quantity of adhesive materials produced by *H. banksii* to affect attachment, and that the quality (attachment performance) of this bioadhesive is comparable to that of other more popular marine organisms such as mussels and barnacles.

Acknowledgements

We acknowledge Tommaso Alestra and David Collings at the School of Biological Sciences at the University of Canterbury (UC) for their help with statistical analysis and staining experiments. Technical assistance for the microfabrication was provided by Helen Devereux and Gary Turner at the Department of Electrical and Computer Engineering at UC. We kindly acknowledge also the biomolecular interaction centre (BIC) at UC for providing internal funding (2014 flagship grant).

Competing interests

The authors have no competing interests.

Author's contributions

SD designed and coordinated the study, participated in data analysis and wrote the manuscript; AM collected the samples, performed the AFM and contact angle measurements,

carried out the flow channel experiments on the various materials, analysed the data and drafted the manuscript; JNU created the topographies and performed the associated flow channel experiments, including contact angle testing; BF carried out the staining experiments; VN helped with the manufacture of the topographies and edited the manuscript.

References

Apple, M. E. and Harlin, M. M. (1995). Inhibition of tetraspore adhesion in *Champia parvula* (Rhodophyta). *Phycologia* **34**, 417–423.

Apple, M. E., Harlin, M. M. and Norris, J. H. (1996). Characterization of *Champia parvula* (Rhodophyta) tetraspore mucilage and rhizoids with histochemical stains and FITC-labelled lectins. *Phycologia* **35**, 245–252.

Arpa-Sancet, M. P., Christophis, C. and Rosenhahn, A., 2012. Microfluidic assay to quantify the adhesion of marine bacteria. *Biointerphases* **7**, 1–9.

Barlow, D. E. and Wahl, K. J. (2012). Optical spectroscopy of marine bioadhesive interfaces. *Annu. Rev. Anal. Chem.* **5**, 229–251.

Bauer, S., Arpa-Sancet, M. P., Finlay, J. A., Callow, M. E., Callow, J. A. and Rosenhahn, A. (2013). Adhesion of marine fouling organisms on hydrophilic and amphiphilic polysaccharides. *Langmuir* **29**, 4039–4047.

Bitton, R., Ben-Yehuda, M., Davidovich, M., Balazs, Y., Potin, P., Delage, L., Colin, C. and Bianco-Peled, H. (2006). Structure of algal-born phenolic polymeric adhesives. *Macromol. Biosci.* **6**, 737–746.

Bouzon, Z. L. and Ouriques, L. C. (2007). Characterization of *Laurencia arbuscula* spore mucilage and cell walls with stains and FITC-labelled lectins. *Aquat. Bot.* **86**, 301–308.

Bråten, T. (1975). Observations on mechanisms of attachment in the green alga *Ulva mutabilis* Føyn. *Protoplasma* **84**, 161–173.

Callow, J. A. and Callow, M. E. (2006). The ulva spore adhesive system. In: *Biological Adhesives* (ed. A. M., Smith and J. A. Callow), pp. 63-78. Berlin, Germany: Springer.

Callow, J. A., Crawford, S. A., Higgins, M. J., Mulvaney, P. and Wetherbee, R. (2000). The application of atomic force microscopy to topographical studies and force measurements on the secreted adhesive of the green alga *Enteromorpha*. *Planta* **211**, 641–647.

Callow, J. A., Stanley, M. S., Wetherbee, R. and Callow, M. E. (2000). Cellular and molecular approaches to understanding primary adhesion in *Enteromorpha*: an overview. *Biofouling* **16**, 141–150.

Callow, J. A., Osborne, M. P., Callow, M. E., Baker, F. and Donald, A. M., 2003. Use of environmental scanning electron microscopy to image the spore adhesive of the marine alga *Enteromorpha* in its natural hydrated state. *Colloids Surf. B Biointerfaces* **27**, 315–321.

Callow, M. E., Evans, L. V., Bolwell, G. P. and Callow, J.A. (1978). Fertilization in brown algae. I. SEM and other observations on fucus serratus. *J. Cell Sci.* **32**, 45–54.

Callow, M. E., Jennings, A. R., Brennan, A. B., Seegert, C. E., Gibson, A., Wilson, L., Feinberg, A., Baney, R. and Callow, J. A. (2002). Microtopographic cues for settlement of zoospores of the green fouling alga *Enteromorpha*. *Biofouling* **18**, 229–236.

Chapman, J. and Regan, F. (2012). Nanofunctionalized superhydrophobic antifouling coatings for environmental sensor applications—Advancing deployment with answers from Nature. *Adv. Eng. Mater.* **14**, B175–B184.

Chiovitti, A., Heraud, P., Dugdale, T. M., Hodson, O. M., Curtain, R. C. A., Dagastine, R. R., Wood, B. R. and Wetherbee, R. (2008). Divalent cations stabilize the aggregation of sulfated glycoproteins in the adhesive nanofibers of the biofouling diatom *Toxarium undulatum*. *Soft Matter* **4**, 811–820.

Dimartino, S., Mather, A. V., Alestra, T., Nawada, S. and Haber, M. (2015). Experimental and computational analysis of a novel flow channel to assess the adhesion strength of sessile marine organisms. *Interface Focus* **5**, 1-12; 20140059.

Dimartino, S., Savory, D. M. and McQuillan, A.J. (2014). Preparation of biological samples for the study of wet-resistant adhesives inspired by kelps. *Proceedings of the 2014 Chemeca Conference*. Perth, WA.

Endrizzi, B. J. and Stewart, R. J. (2009). Glueomics: an expression survey of the adhesive gland of the sandcastle worm. *J. Adhes*. **85**, 546–559.

Fagerberg, W. R., Towle, J., Dawes, C. J. and Böttger, A. (2012). Bioadhesion in *Caulerpa mexicana* (chlorophyta): rhizoid-substrate adhesion. *J. Phycol.* **48**, 264–269.

Forbes, M. A. and Hallam, N.D. (1979). Embryogenesis and substratum adhesion in the brown alga *Hormosira banksii* (Turner) Decaisne. *Br. Phycol. J.* **14**, 69–81.

Frazer, R. Q., Byron, R. T., Osborne, P. B. and West, K. P. (2005). PMMA: an essential material in medicine and dentistry. *J. Long. Term Eff. Med. Implants* **15**, 629–639.

Granhag, L., Finlay, J., Jonsson, P., Callow, J. A., Callow, M. E. (2004). Roughness-dependent removal of settled spores of the green alga *Ulva* (syn. *Enteromorpha*) exposed to hydrodynamic forces from a water jet. *Biofouling* **20**, 117–122.

Haller, C. M., Buerzle, W., Brubaker, C. E., Messersmith, P. B., Mazza, E., Ochsenbein-Koelble, N., Zimmermann, R. and Ehrbar, M. (2011). Mussel-mimetic tissue adhesive for

fetal membrane repair: a standardized ex vivo evaluation using elastomeric membranes. *Prenat. Diagn.* **31**, 654–660.

Harder, D. L., Hurd, C. L. and Speck, T. (2006). Comparison of mechanical properties of four large, wave-exposed seaweeds. *Am. J. Bot.* **93**, 1426–1432.

Hennebert, E., Wattiez, R., Waite, J. H. and Flammang, P. (2012). Characterization of the protein fraction of the temporary adhesive secreted by the tube feet of the sea star *Asterias rubens*. *Biofouling* **28**, 289–303.

Hodson, O. M., Monty, J. P., Molino, P. J. and Wetherbee, R. (2012). Novel whole cell adhesion assays of three isolates of the fouling diatom *Amphora coffeaeformis* reveal diverse responses to surfaces of different wettability. *Biofouling* **28**, 381–393.

Hong, T. F., Ju, W. J., Wu, M. C., Tai, C. H., Tsai, C. H. and Fu, L. M. (2010)**.** Rapid prototyping of PMMA microfluidic chips utilizing a CO_2 laser. *Microfluid. Nanofluidics* **9**, 1125–1133.

Jordan, P. and Vilter, H. (1991). Extraction of proteins from material rich in anionic mucilages: Partition and fractionation of vanadate-dependent bromoperoxidases from the brown algae *Laminaria digitata* and *L. saccharina* in aqueous polymer two-phase systems. *Biochim. Biophys. Acta BBA - Gen. Subj.* **1073**, 98–106.

Lee, H., Dellatore, S. M., Miller, W. M. and Messersmith, P. B. (2007). Mussel-inspired surface chemistry for multifunctional coatings. *Science* **318**, 426–430.

Levi, B. and Friedlander, M. (2004). Identification of two putative adhesive polypeptides in *Caulerpa prolifera* rhizoids using an adhesion model system. *J. Appl. Phycol.* **16**, 1–9.

Long, C. J., Schumacher, J. F., Robinson, P. A. C., Finlay, J. A., Callow, M. E., Callow, J. A. and Brennan, A. B. (2010). A model that predicts the attachment behavior of *Ulva linza* zoospores on surface topography. *Biofouling* **26**, 411–419.

Petrone, L., Di Fino, A., Aldred, N., Sukkaew, P., Ederth, T., Clare, A. S. and Liedberg, B. (2011). Effects of surface charge and Gibbs surface energy on the settlement behaviour of barnacle cyprids (*Balanus amphitrite*). *Biofouling* **27**, 1043–55.

McKenzie, P. F. and Bellgrove, A. (2009). Dislodgment and attachment strength of the intertidal macroalga *Hormosira banksii* (Fucales, Phaeophyceae). *Phycologia* **48**, 335–343.

Molino, P. J., Hodson, O. M., Quinn, J. F. and Wetherbee, R. (2008). The quartz crystal microbalance: a new tool for the investigation of the bioadhesion of diatoms to surfaces of differing surface energies. *Langmuir* **24**, 6730–6737.

Molino, P. J., Hodson, O. M., Quinn, J. F. and Wetherbee, R. (2006). Utilizing QCM-D to characterize the adhesive mucilage secreted by two marine diatom species in-situ and in real-time. *Biomacromolecules* **7**, 3276–3282.

Moss, B. (1975). Attachment of zygotes and germlings of *Ascophyllum nodosum* (L.) Le Jol. (Phaeophyceae, Fucales). *Phycologia* **14**, 75–80.

Myan, F. W. Y., Walker, J. and Paramor, O. (2013). The interaction of marine fouling organisms with topography of varied scale and geometry: a review. *Biointerphases* **8**, 1–13.

Norton, T. A. (1983). The resistance to dislodgement of *Sargassum muticum* germlings under defined hydrodynamic conditions. *J. Mar. Biol. Assoc. U. K.* **63**, 181–193.

Onda, T., Shibuichi, S., Satoh, N. and Tsujii, K. (1996). Super-water-repellent fractal surfaces. *Langmuir* **12**, 2125–2127.

Osborn, J. E. M. (1948). The Structure and Life History of *Hormosira banksii* (Turner) Decaisne. *Trans. Proc. R. Soc. N. Z.* **77**, 47–71.

Ouriques, L. C., Schmidt, É. C. and Bouzon, Z. L. (2012). The mechanism of adhesion and germination in the carpospores of *Porphyra spiralis* var. *amplifolia* (Rhodophyta, Bangiales). *Micron* **43**, 269–277.

Petrone, L. (2013). Molecular surface chemistry in marine bioadhesion. *Adv. Colloid Interface Sci.* **195-196**, 1–18.

Petrone, L., Easingwood, R., Barker, M. F. and McQuillan, A. J. (2011). In situ ATR-IR spectroscopic and electron microscopic analyses of settlement secretions of *Undaria pinnatifida* kelp spores. *J. R. Soc. Interface* **8**, 410–422.

Pettitt, M. E., Henry, S. L., Callow, M. E., Callow, J. A. and Clare, A.S. (2004). Activity of commercial enzymes on settlement and adhesion of cypris larvae of the barnacle *Balanus amphitrite*, apores of the green alga *Ulva linza*, and the diatom *Navicula perminuta*. *Biofouling* **20**, 299–311.

Cox, R. A., McCartney, M. J. and Culkin, F. (1970). The specific gravity/salinity/temperature relationship in natural sea water. *Deep Sea Res. Oceanogr. Abstr.* **17**, 679–689.

Rosenhahn, A., Finlay, J., Pettit, M., Ward, A., Wirges, W., Gerhard, R., Callow, M. E., Grunze, M. and Callow, J. A. (2009). Zeta potential of motile spores of the green alga *Ulva linza* and the influence of electrostatic interactions on spore settlement and adhesion strength. *Biointerphases* **4**, 7–11.

Rosenhahn, A. and Sendra, G. H. (2012). Surface sensing and settlement strategies of marine biofouling organisms. *Biointerphases* **7**, 1–13.

Santos, R., Aldred, N., Gorb, S. and Flammang, P. (2013). *Biological and Biomimetic Adhesives*. Cambridge, UK: Royal Society of Chemistry Publishing.

Schultz, M. P., Finlay, J. A., Callow, M. E. and Callow, J. A. (2000). A turbulent channel flow apparatus for the determination of the adhesion strength of microfouling organisms. *Biofouling* **15**, 243–251.

Seymour, R. J., Tegner, M. J., Dayton, P. K. and Parnell, P. E. (1989). Storm wave induced mortality of giant kelp, *Macrocystis pyrifera*, in Southern California. *Estuar. Coast. Shelf Sci.* **28**, 277–292.

Sridharan, G. and Shankar, A. A. (2012). Toluidine blue: A review of its chemistry and clinical utility. *J. Oral Maxillofac. Pathol.* **16**, 251–255.

Stewart, R. J., Ransom, T. C., Hlady, V. (2011). Natural underwater adhesives. *J. Polym. Sci. Part B Polym. Phys.* **49**, 757–771.

Suci, P. A. and Geesey, G. G. (2001). Comparison of adsorption behavior of two *Mytilus edulis* foot proteins on three surfaces. *Colloids Surf. B Biointerfaces* **22**, 159–168. doi:10.1016/S0927-7765(01)00149-7

Sun, M., Luo, C., Xu, L., Ji, H., Ouyang, Q., Yu, D. and Chen, Y. (2005). Artificial lotus leaf by nanocasting. *Langmuir* **21**, 8978–8981.

Tarakhovskaya, E. R. (2014). Mechanisms of bioadhesion of macrophytic algae. *Russ. J. Plant Physiol.* **61**, 19–25.

Taylor, D. I., Delaux, S., Stevens, C., Nokes, R. and Schiel, D. R. (2010). Settlement rates of macroalgal algal propagules: Cross-species comparisons in a turbulent environment. *Limnol. Oceanogr.* **55**, 66–76.

Taylor, D. I. and Schiel, D. R. (2003). Wave-related mortality in zygotes of habitat-forming algae from different exposures in southern New Zealand: the importance of 'stickability'. *J. Exp. Mar. Biol. Ecol.* **290**, 229–245.

Vreeland, V. and Epstein, L. (1996). Analysis of plant-substratum adhesives, in *Modern Methods of Plant Analysis* (ed. H. F. Linskens and J. F. Jackson), pp. 95–116. Berlin: Springer-Verlag.

Waite, J. H. and Qin, X. (2001). Polyphosphoprotein from the adhesive pads of mytilus edulis. *Biochemistry* **40**, 2887–2893.

Walker, G. C., Sun, Y., Guo, S., Finlay, J. A., Callow, M. E. and Callow, J. A. (2005). Surface mechanical properties of the spore adhesive of the green alga *Ulva*. *J. Adhes.* **81**, 1101–1118.

Weaver, K. D., Stoffer, J. O. and Day, D. E. (1993). Preparation and properties of optically transparent, pressure-cured poly(methacrylate) composites. *Polym. Compos.* **14**, 515–523.

Figure captions

Figure 1: Microscopy images of H. banksii germlings stained with toluidine blue after 6 (A), 12 (B), 24 (C), and 96 h (D) following fertilization. Scale bars correspond to 20 µm. In the background is visible the excess sperm added to fertilize the eggs.

Figure 2: Initial settlement density, D0, for H. banksii germlings over the different substrates at each settlement time (± S.E., n = 3).

Figure 3: H. banksii germling survival with increasing fluid velocity/shear pressure for different settlement times on the different substrates (± S.E., n = 3).

Figure 4: S2.5 for H. banksii germlings at the various settlement times. Note, at 12 h settlement time S2.5 was zero across all the different substrates and thus not reported (± S.E., n = 3).

Figure 5: Settlement patterning of H. banksii germlings 24 hours post-settlement. (A) Control (flat) surface, (B) 40 µm, (C) 80 µm and (D) 160 µmgrooved surfaces. Circles indicate examples where clustering of germlings has resulted in germlings settling on a ridge between two grooves. Scale bars correspond to 500 µm.

Figure 6: Initial settlement density, D0, for H. banksii germlings over the different textured substrates at increasing settlement times (± S.E., n = 3).

Figure 7: Survival rate of H. Banksii germlings vs fluid velocity for the various topographies tested and at the different settlement times (± S.E., n = 3).

Figure 8: Series of frames showing the detachment of H. banksii germlings settled for 96 h during the flow channel experiments. Flow velocities: (A) = 0.83 m/s, (B) = 1.25 m/s, (C) = 1.67 m/s, (D) = 2.08 m/s. Scale bars correspond to 100 µm. Black arrow: germling revolving around fixed point at end of the rhizoid before detachment. Yellow arrows: other germlings partially rotating around rhizoidal tip.

673 Figure 9: Representations of spherical bodies with 80 µm dimaeter settled on (a) 40 µm
674 groove, (b) 80 µm groove, (c) 160 µm groove and (d) flat surface.
675

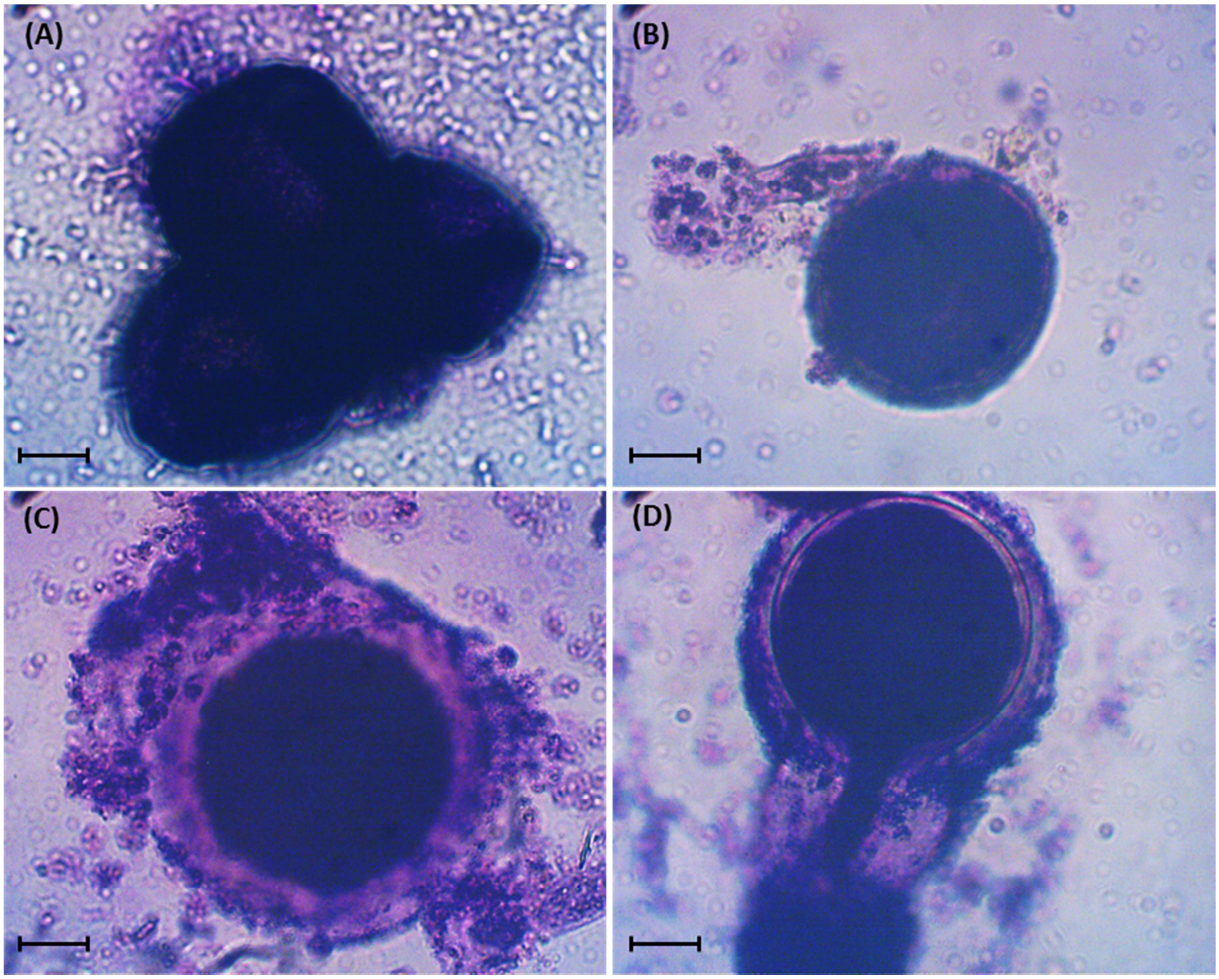

Figure 1: Microscopy images of *H. banksii* germlings stained with toluidine blue after 6 (A), 12 (B), 24 (C), and 96 h (D) following fertilization. Scale bars correspond to 20 µm. In the background is visible the excess sperm added to fertilize the eggs.

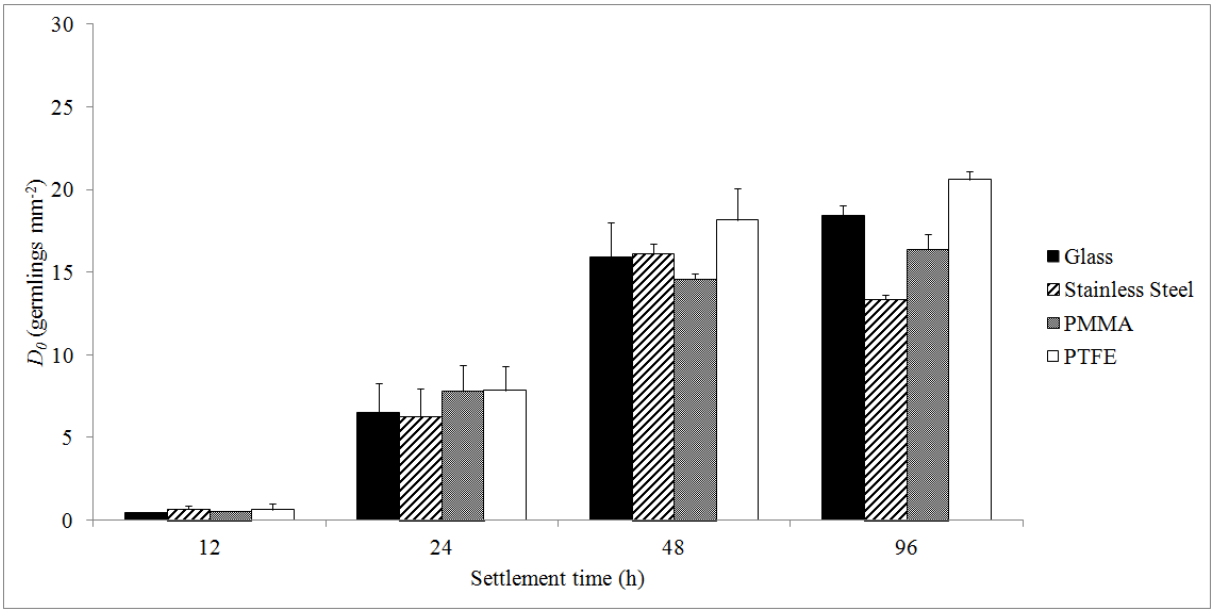

681

682 **Figure 2: Initial settlement density, D_0, for *H. banksii* germlings over the different**
683 **substrates at each settlement time (± S.E., n = 3).**

684

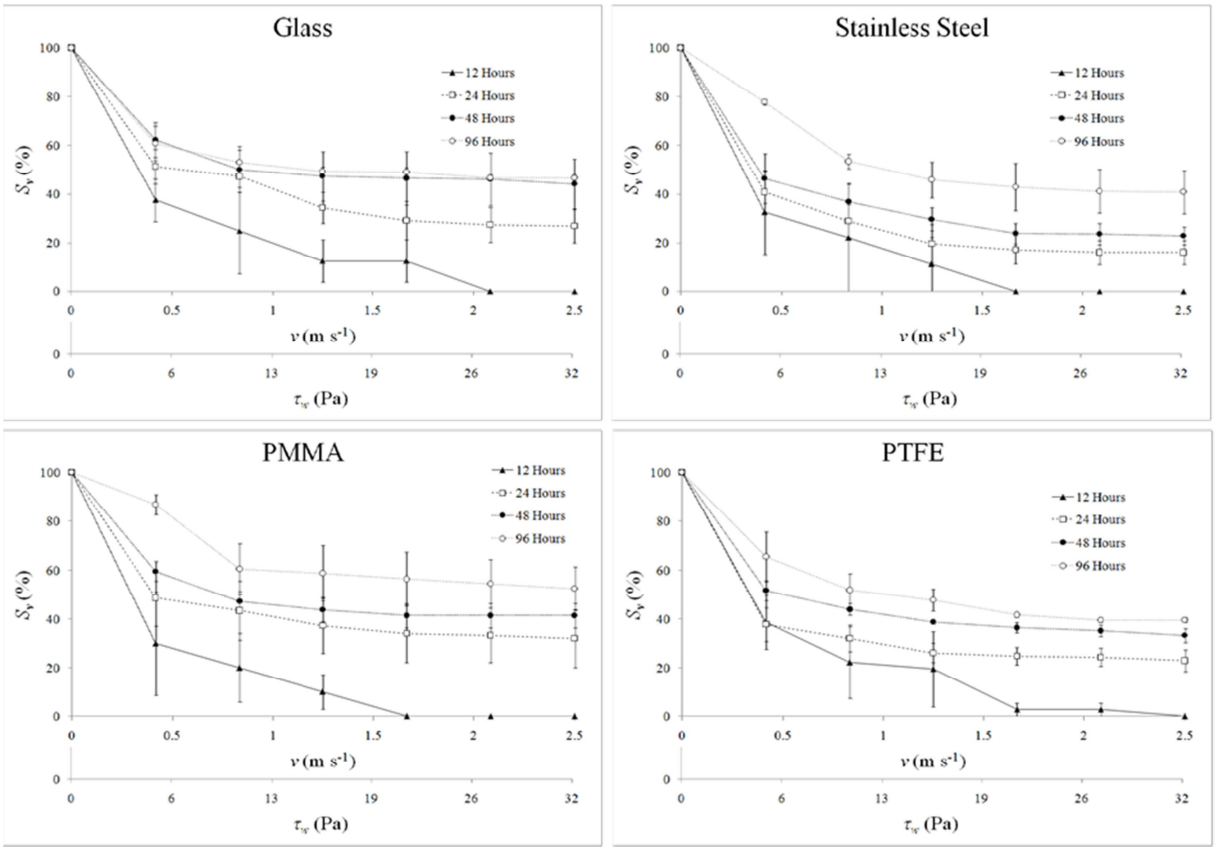

685

686 **Figure 3: *H. banksii* germling survival with increasing fluid velocity/shear pressure for**
687 **different settlement times on the different substrates (± S.E., n = 3).**

688

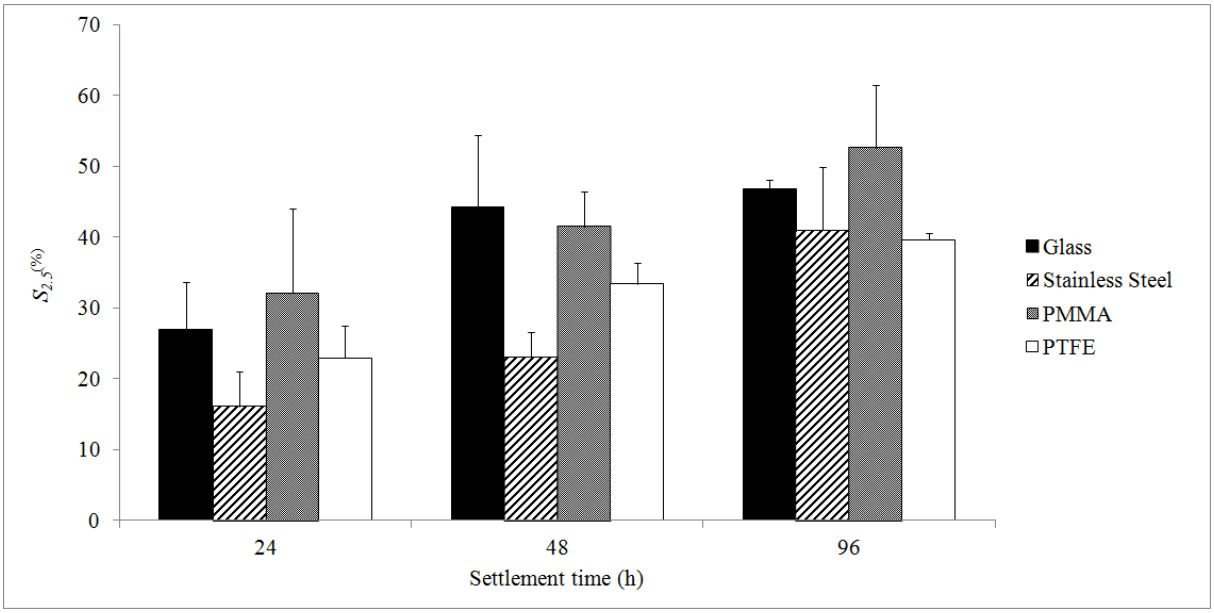

689

690 Figure 4: $S_{2.5}$ for *H. banksii* germlings at the various settlement times. Note, at 12 h settlement
691 time $S_{2.5}$ was zero across all the different substrates and thus not reported (± S.E., n = 3).

692

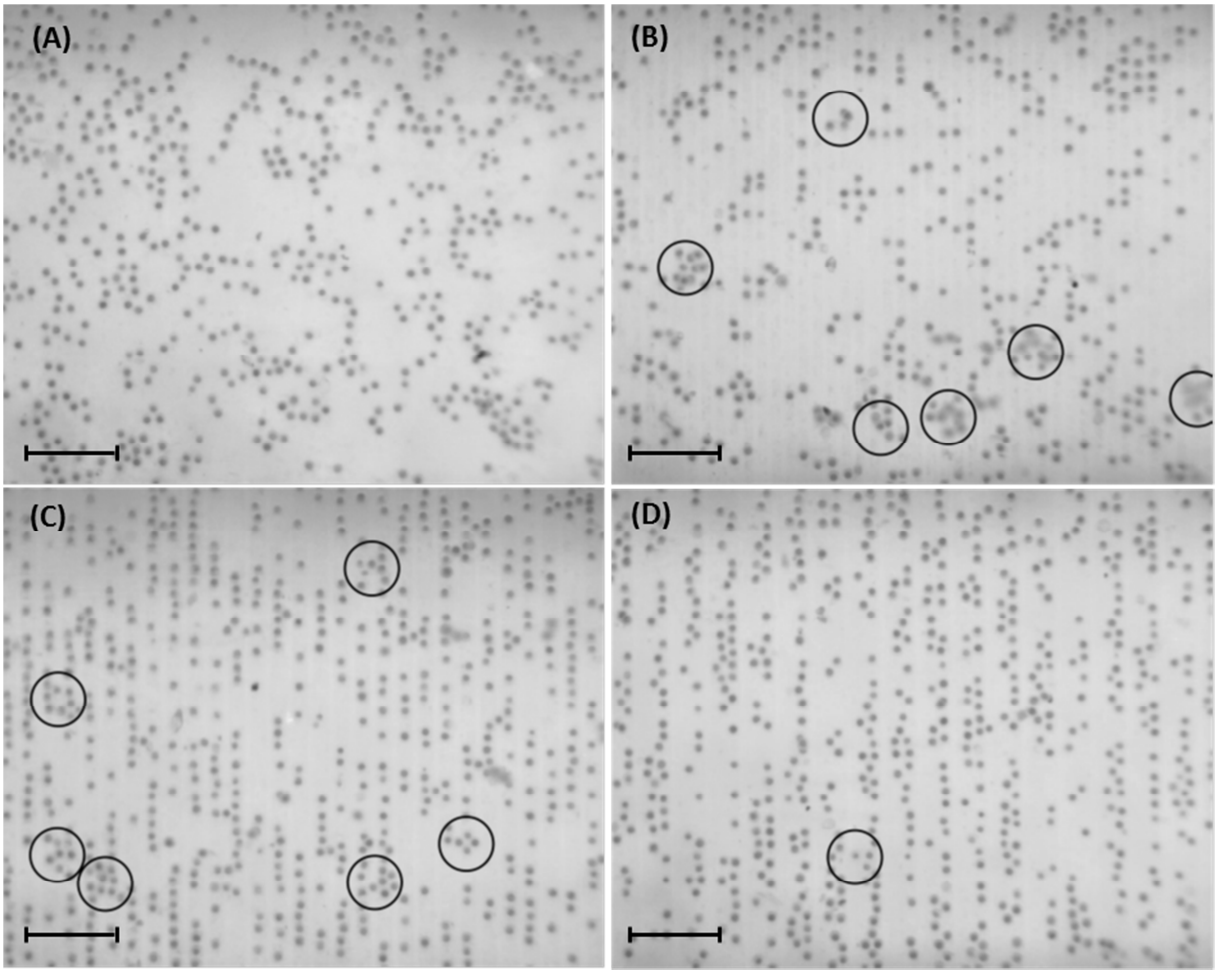

Figure 5: Settlement patterning of *H. banksii* germlings 24 hours post-settlement. (A) Control (flat) surface, (B) 40 µm, (C) 80 µm and (D) 160 µm grooved surfaces. Circles indicate examples where clustering of germlings has resulted in germlings settling on a ridge between two grooves. Scale bars correspond to 500 µm.

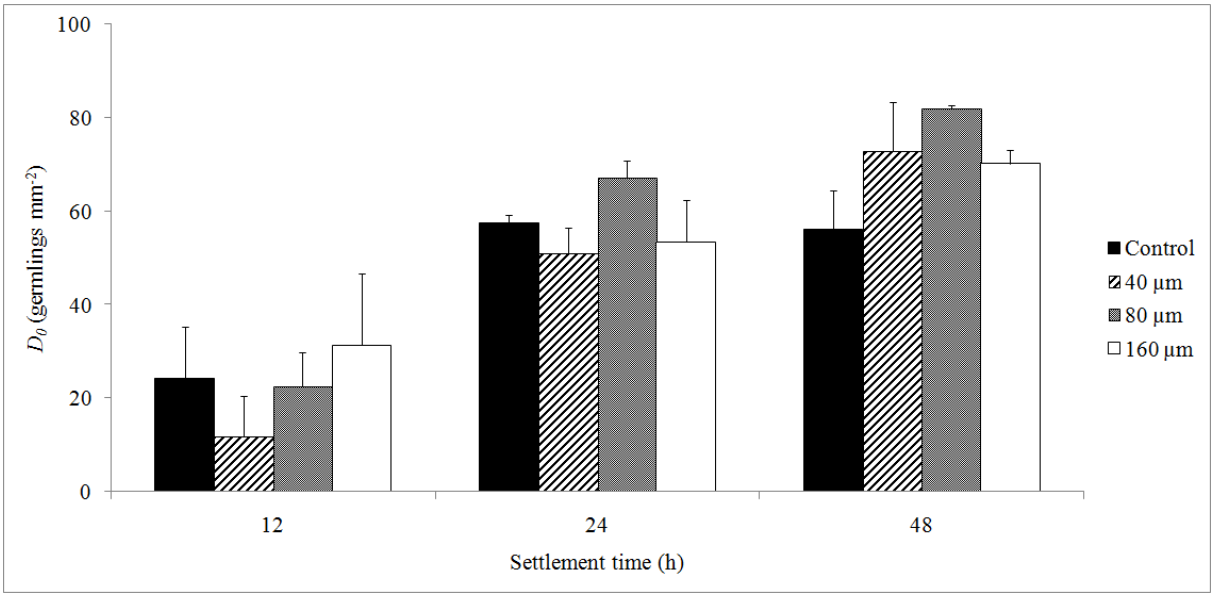

Figure 6: Initial settlement density, D_0, for *H. banksii* germlings over the different textured substrates at increasing settlement times (± S.E., n = 3).

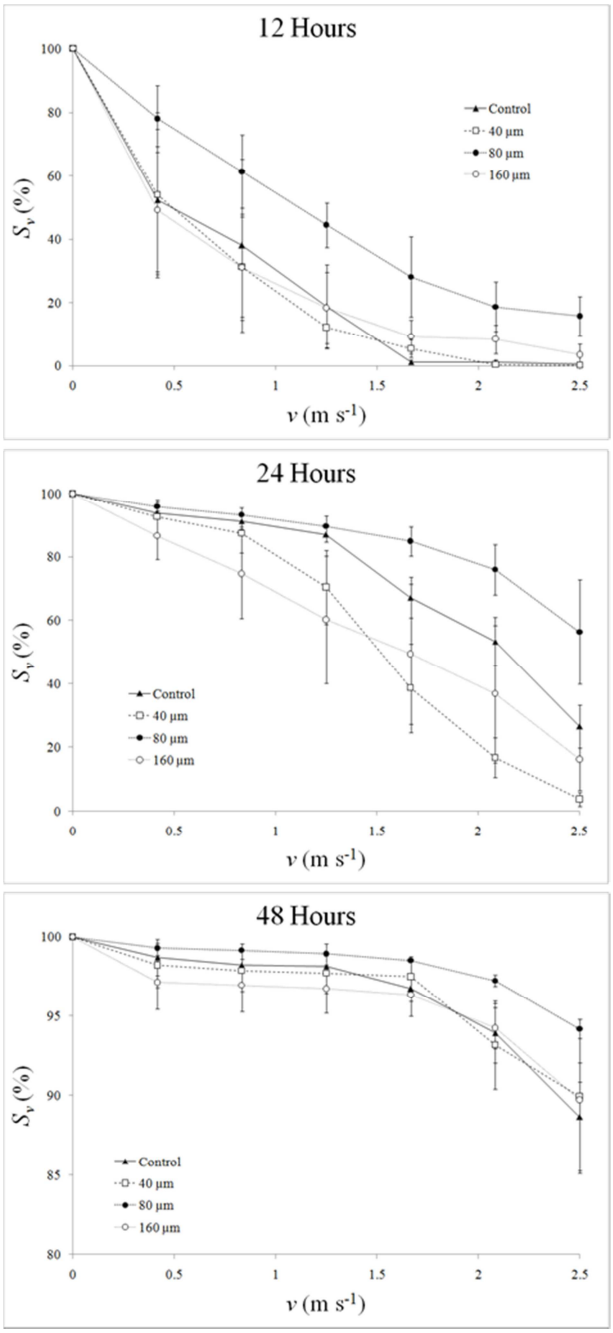

Figure 7: Survival rate of *H. Banksii* germlings vs fluid velocity for the various topographies tested and at the different settlement times (± S.E., n = 3).

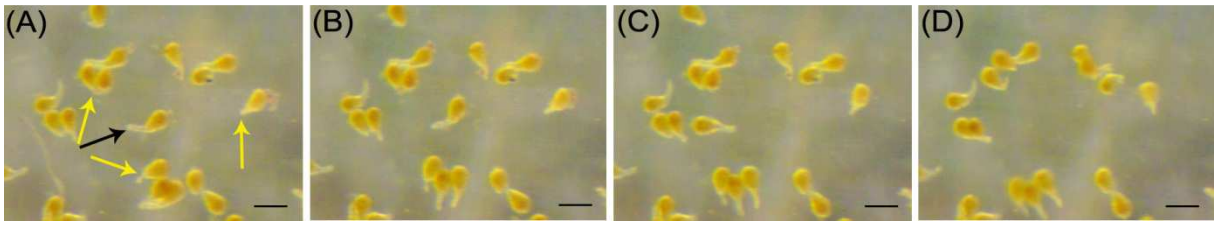

Figure 8: Series of frames showing the detachment of *H. banksii* germlings settled for 96 h during the flow channel experiments. Flow velocities: (A) = 0.83 m/s, (B) = 1.25 m/s, (C) = 1.67 m/s, (D) = 2.08 m/s. Scale bars correspond to 100 µm. Black arrow: germling revolving around fixed point at end of the rhizoid before detachment. Yellow arrows: other germlings partially rotating around rhizoidal tip.

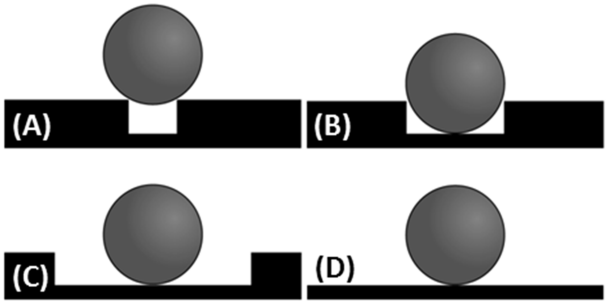

Figure 9: Representations of spherical bodies with 80 µm diameter settled on (a) 40 µm groove, (b) 80 µm groove, (c) 160 µm groove and (d) flat surface.